Dynamic Cooperative Energy and Coverage Management for V2G-Enhanced RAN Resilience

Dynamic Cooperative Energy and Coverage Management for V2G-Enhanced RAN Resilience

Mohammad Reza Jokar[1], Aurora Martiny[1], and Michela Meo[1]

[1]*Department of Electronics and Telecommunications, Politecnico di Torino*, Turin, Italy
Emails: {mohammadreza.jokar, aurora.martiny, michela.meo}@polito.it

***Abstract*—The resilience of cellular communication is paramount, given how widely its services are used. However, it also depends on the resilience of the power grid, which is increasingly threatened by extreme weather events and the growing reliance on distributed, intermittent energy sources. Current base station backup systems, typically limited to 2-6 hours of autonomy, operate in isolation and fail to leverage spatial redundancy. This paper proposes the Multi-Site Resiliency Cooperative (MSRC) framework, a unified control strategy that transforms independent sites into a collaborative energy cluster. We formulate a two-stage mixed-integer optimization problem that jointly manages radio coverage adaptation switching sites between helping, assisted, and deep-sleep modes and dynamic Vehicle-to-Grid (V2G) energy injection. By proactively reshaping cell boundaries and traffic loads based on real-time battery states, MSRC maximizes network survival while prioritizing critical service classes. Extensive simulations on a 19-site urban network demonstrate that the proposed framework extends survival time by 96% and maintains 94% service continuity compared to conventional baselines. Crucially, MSRC requires no physical infrastructure upgrades, offering operators a deployable, software-defined solution for outage-resilient green communications.**

***Index Terms*—Energy management, cooperative communications, MILP optimization, vehicle-to-grid, RAN resilience, green networking.**

I. Introduction

Mobile networks have evolved into critical lifeline infrastructure, and advancements in Radio Access Networks (RANs) necessitate high levels of operational resilience. However, their resilience remains fundamentally constrained by dependence on a stable power grid. Grid failures routinely overwhelm the limited 2-6 h autonomy of on-site base station (BS) batteries [1], as demonstrated during the April 2025 Iberian Peninsula blackout, where more than 50% of mobile subscribers lost service [2]. This gap between backup capacity and outage duration is widening: major grid failures increasingly last many hours, driven by the intensifying frequency of extreme-weather events and a structural mismatch between the projected surge in electricity demand and the slow reinforcement of distribution networks [3]. Unmanaged Electric Vehicles (EVs) charging alone is expected to increase regional peak loads by 15-20%, further stressing already constrained grids [4]. Conventional hardening strategies, including diesel generators, renewable-powered sites, or hybrid backup architectures, face significant limitations: while renewable solutions offer green alternatives, they remain intermittent, whereas diesel systems are both carbon-intensive and costly. Meanwhile, existing RAN-side mechanisms improve spectral efficiency but treat BSs as isolated energy entities, overlooking the potential for inter-site cooperation [5] [6]. As a result, adjacent BSs often fail simultaneously despite having complementary traffic and battery conditions.

A growing body of research explores energy-efficient BS sleep modes and Vehicle-to-Grid (V2G) or Vehicle-to-Everything (V2X) strategies. With the global EV fleet expected to exceed 145 million by 2030 [7], EV batteries represent a massive and geographically distributed energy resource. However, existing works address these components in isolation. EV-to-BS emergency power-supply models focus on EV routing logistics while assuming independent BS operation, and therefore do not consider radio coverage, cooperative sleep modes, or joint traffic offloading mechanisms [8]. Likewise, digital-twin-based EV-BS energy-exchange frameworks optimize buyer-seller matching but ignore RAN coupling, coverage reshaping, or joint user-association and carrier-activation decisions [9].

To the best of our knowledge, no study provides a cohesive framework that jointly coordinates BSs, stationary batteries, and EVs under outage conditions while preserving radio-coverage guarantees. To bridge this gap, this paper proposes the *Multi-Site Resiliency Cooperative (MSRC)* framework. Unlike traditional disjoint management, MSRC optimizes the interaction among a cluster of BSs, which act as a cohesive energy microgrid, balancing coverage requirements against real-time battery levels to maximize network survival.

The specific contributions of this work are as follows:

- **Coverage Cooperation Logic:** We introduce a four-state operational model (Normal, Helping, Assisted, Deep-Sleep) that allows sites to dynamically reshape coverage boundaries to offload traffic from energy-poor neighbors.
- **Joint MILP Formulation:** We develop a Mixed-Integer Linear Programming (MILP) formulation that simultaneously optimizes user association, carrier activation, and V2G injection, ensuring radio resource decisions are driven by energy survival targets.
- **Hierarchical Control Architecture:** To ensure computational scalability, we design a two-layer control strategy that decouples slow-timescale cooperative planning from fast-timescale radio resource allocation, making the system deployable in real-time scenarios.

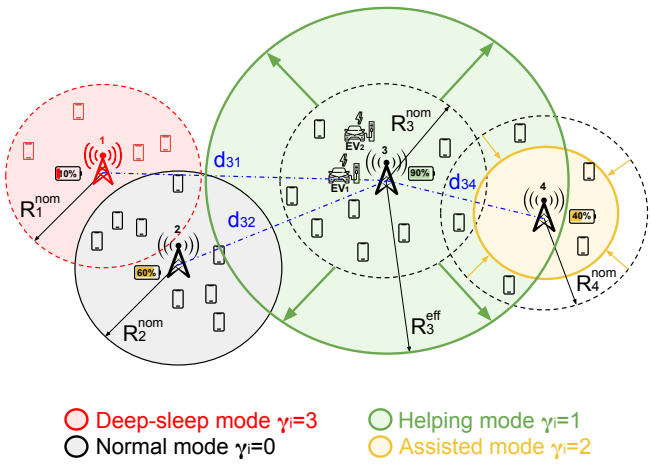

Fig. 1. MSRC cooperation modes (normal, helping, assisted, deep-sleep) and the resulting coverage regions in a four-site cluster.

II. System Model

A. Network Architecture and Cooperation Framework

We consider a geographic region where a cellular network comprises N BSs, indexed by $\mathcal{N}$. Each station $i \in \mathcal{N}$ at position $\mathbf{p}_i = (x_i, y_i)$ serves users within a nominal coverage region $\mathcal{A}_i^{\text{nom}}$, modeled as a disk of nominal radius R_i^{nom}. When a power failure occurs at instant t_0, each BS switches to battery-powered operation. To extend service availability beyond the limits of individual batteries, we enable strategic cooperation among geographically near stations according to four possible modes (Fig. 1): *normal* ($\gamma_i = 0$), *helping* ($\gamma_i = 1$), *assisted* ($\gamma_i = 2$), and *deep-sleep* ($\gamma_i = 3$). In particular, normal mode serves nominal coverage $\mathcal{A}_i^{\text{nom}}$; helping mode expands coverage up to $\mathcal{A}_i^{\text{exp}}$ to serve neighboring traffic; assisted mode offloads traffic; deep-sleep deactivates all bands. We define a cooperation graph $\mathcal{G} = (\mathcal{N}, \mathcal{E})$, where edge $(i, j) \in \mathcal{E}$ indicates that stations i and j can coordinate operations when their distance $d_{ij} = \|\mathbf{p}_i - \mathbf{p}_j\|_2 \le R_{\text{coop}}$, and R_{coop} is selected yo ensure that neighboring stations have non-negligible coverage overlap. We quantify apriori the assistance potential κ_{ij} as:

$$\kappa_{ij} = \frac{|\mathcal{A}_i^{\text{exp}} \cap \mathcal{A}_j^{\text{nom}}|}{|\mathcal{A}_j^{\text{nom}}|}, \tag{1}$$

where $\mathcal{A}_i^{\text{exp}}$ is the expanded coverage. Note that $\mathcal{G}$ is undirected, while κ_{ij} is directional ($\kappa_{ij} \neq \kappa_{ji}$). Performance is benchmarked against two baselines:

- *Independent Operation:* BSs operate autonomously without radio cooperation ($\gamma_i = 0$), though sites may still utilize local V2G energy if an EV is present.
- *Static Load Balancing:* nearby BSs expand coverage based on fixed rules without dynamic energy-aware adaptation.

B. Power Consumption Model with Cooperation Modes

1) Baseline Power Model: The power consumption of sector s operating on band $b \in \mathcal{B}_i$ at site i follows the linear model from [10]:

$$\begin{aligned} P_{i,s}^{(b)}(t) = \beta_0^{(b)} + \beta_1^{(b)} \rho_{\text{DL}}^{(b)}(t) + \beta_2^{(b)} \rho_{\text{UL}}^{(b)}(t) + \beta_3^{(b)} \nu_{\text{DL}}^{(b)}(t) \\ + \beta_4^{(b)} \nu_{\text{UL}}^{(b)}(t) + \beta_5^{(b)} P_{\text{tx}}^{(b)} + \beta_6^{(b)} \mathcal{L}^{(b)}, \end{aligned} \tag{2}$$

where $\rho_{\text{DL/UL}}^{(b)}(t)$ denotes Resource-Block (RB) utilization, $\nu_{\text{DL/UL}}^{(b)}(t)$ is traffic volume, $P_{\text{tx}}^{(b)}$ is transmit power, $\mathcal{L}^{(b)}$ represents feeder losses, and $\{\beta_k^{(b)}\}$ are calibrated coefficients. This linear formulation enables efficient MILP optimization while capturing both static and load-dependent components.

2) Cooperation Modes: Under cooperation, the traffic volumes considered in (2) become the effective traffic $\nu_{*,\text{eff}}^{(b)}(t)$, representing the total load handled by the site. For each band b, $\nu_{\text{DL}}^{(b)}(t)$ is updated as:

$$\begin{aligned} \nu_{\text{DL,eff}}^{(b)}(t) &= \nu_{\text{DL}}^{(b)}(t) + \Delta\nu_{\text{DL,help}}^{(b)}(t) - \Delta\nu_{\text{DL,off}}^{(b)}(t), \\ \nu_{\text{UL,eff}}^{(b)}(t) &= \nu_{\text{UL}}^{(b)}(t) + \Delta\nu_{\text{UL,help}}^{(b)}(t) - \Delta\nu_{\text{UL,off}}^{(b)}(t), \end{aligned} \tag{3}$$

where $\Delta\nu_{\text{help}}^{(b)}$ is the added traffic when helping and $\Delta\nu_{\text{off}}^{(b)}$ is the load subtracted due to successful offloading to a neighbor. RB utilization is assumed to scale linearly: $\rho_{\text{eff}}^{(b)} = \rho^{(b)} \cdot (\nu_{\text{eff}}^{(b)} / \nu^{(b)})$. Substituting these values into (2) yields the mode-dependent power without the need for predefined scaling factors. The total site power aggregates active bands and mode-specific consumption:

$$\begin{aligned} P_i^{\text{total}}(t) = \sum_{b \in \mathcal{B}_i} \sum_{s \in \mathcal{S}_i} z_i^{(b)}(t)\, P_{i,s}^{(b)}(t) \\ + P_{\text{sleep}} \mathbb{1}[\gamma_i(t) = 3] + \sum_{b \in \mathcal{B}_i} (1 - z_i^{(b)}(t)) P_{\text{std}}^{(b)}, \end{aligned} \tag{4}$$

where $z_i^{(b)}(t) \in \{0, 1\}$ activates band b and $P_{\text{std}}^{(b)}$ is standby power. In deep-sleep ($\gamma_i = 3$), all bands power down ($z_i^{(b)} = 0, P_{\text{std}}^{(b)} = 0$), leaving only $P_{\text{sleep}} \approx 100$ W active, consistent with standard 3GPP micro-sleep state-4 specifications.

C. Dynamic Coverage and User Association

The cooperation modes defined in Sec. II-B dynamically adapt each BS's coverage and user assignment (Fig. 1), which determines the traffic load in Eq. (2).

1) Coverage Adaptation: Unlike conventional fixed-coverage approaches, our framework exploits the frequency-dependent propagation characteristics of multi-band systems to enable energy-efficient spatial adaptation. Each band $b \in \mathcal{B}_i$ provides a distinct $R_i^{\text{nom}(b)}$, which is formally defined as the maximum distance where the received SINR (determined by 3GPP models [11]) satisfies the minimum decoding threshold $\Gamma_{\min}$. This creates a natural coverage hierarchy where lower frequencies (e.g., 800 MHz) extend significantly farther than higher-capacity bands (e.g., 3.7 GHz) [12]. The effective coverage radius R^{eff} adapts based on the cooperation mode, where transitions between modes are triggered by the site's

instantaneous State-of-Charge (SoC) and the localized traffic demand:

$$R_i^{\text{eff}}(t) = \begin{cases} \max_{b\in\mathcal{B}_i}\{z_i^{(b)}(t)R_i^{\text{nom}(b)}\}, & \gamma_i(t)=0, \\ R_i^{\text{nom}(b_{\max})}, & \gamma_i(t)=1, \\ R_i^{\text{nom}(b_{\min})}, & \gamma_i(t)=2, \\ 0, & \gamma_i(t)=3, \end{cases} \tag{5}$$

where $b_{\max}$ and $b_{\min}$ identify the bands with maximum and minimum propagation reach, respectively. In helping mode ($\gamma_i = 1$), the station activates its lowest-frequency band to maximize spatial reach; in assisted mode ($\gamma_i = 2$), it restricts operation to higher bands, reducing coverage to save energy while maintaining capacity for proximate users.

User u at location $\mathbf{q}_u$ can connect to BS i if spatial proximity and signal quality requirements are jointly satisfied:

$$\|\mathbf{q}_u - \mathbf{p}_i\|_2 \le R_i^{\text{eff}}(t) \quad \text{and} \quad \max_{b\in\mathcal{B}_i} \text{SINR}_{i,u}^{(b)}(t) \ge \Gamma_{\min}, \tag{6}$$

where the received SINR on band b accounts for path gain $G_{i,u}^{(b)}$, noise power σ^2, and interference from active neighboring sites:

$$\text{SINR}_{i,u}^{(b)}(t) = \frac{P_{\text{tx}}^{(b)} G_{i,u}^{(b)}}{\sigma^2 + \sum_{j\neq i,\gamma_j\neq 3} P_{\text{tx}}^{(b)} G_{j,u}^{(b)}}. \tag{7}$$

2) User Association and Rate Allocation: Each user associates with exactly one feasible BS through binary assignment variables $x_{i,u}(t) \in \{0,1\}$ such that $\sum_{i\in\mathcal{N}} x_{i,u}(t) = 1$. The achievable rate $r_{i,u}(t)$ follows Shannon capacity across all active bands:

$$r_{i,u}(t) = \sum_{b\in\mathcal{B}_i} z_i^{(b)}(t)\, B^{(b)} \log_2\Big(1 + \text{SINR}_{i,u}^{(b)}(t)\Big)\, \chi_{i,u}^{(b)}(t), \tag{8}$$

where $B^{(b)}$ is the bandwidth and $\chi_{i,u}^{(b)}(t) \in [0,1]$ represents the fraction of band resources allocated to user u, constrained by the physical budget: $\sum_u \chi_{i,u}^{(b)}(t) \le 1$.

3) Capacity and Service Classes: The aggregate served traffic at site i is bounded by its instantaneous capacity:

$$\sum_{u:x_{i,u}(t)=1} r_{i,u}(t) \le \sum_{b\in\mathcal{B}_i} z_i^{(b)}(t)\, C^{(b)}\, (1 - \lambda_{\text{loss}}\mathbb{1}[\gamma_i(t)=1]), \tag{9}$$

where $C^{(b)}$ is the nominal band capacity and $\lambda_{\text{loss}} \approx 0.05$ accounts for scheduling overhead. Users are stratified into classes $\mathcal{U}$ with priority weights $w_u \in \{1000, 100, 10, 1\}$ used to penalize traffic drops in the objective. Each user u specifies a throughput demand $D_u(t)$ (the requested Mbps) and a minimum rate $R_u^{\min}$ enforced via Service-Level Agreements (SLA):

$$r_{i,u}(t) \ge R_u^{\min}, \quad \forall u \in \mathcal{U}\setminus\mathcal{U}^{\text{be}},\ t\in\mathcal{T}. \tag{10}$$

4) Link to Power Model: The user association and rate allocation decisions determine aggregate traffic metrics that close the modeling loop:

$$\nu_{\text{DL}}^{(b)}(t) = \sum_u r_{i,u}(t), \quad \rho_{\text{DL}}^{(b)}(t) = \sum_u \chi_{i,u}^{(b)}(t). \tag{11}$$

These quantities feed into Eq. (3) to update power consumption in (2), completing the dynamic coupling between cooperation decisions and energy utilization.

D. Energy Storage and EV-Assisted Operation

Each site is equipped with a stationary battery energy storage system (BESS) and a bidirectional V2G charger that enables energy exchange with connected EVs. During grid outages, the BESS supplies the local load; when excess EV energy is available, it can also be recharged from the fleet. Long-term degradation is neglected, as the analysis focuses on short operational windows.

1) Stationary Battery Dynamics: The BESS state of charge (SoC) evolves as

$$\text{SOC}_i^{t+1} = \text{SOC}_i^t + \frac{\eta_{\text{ch}} P_{\text{ch},i}^t \Delta t}{E_{\text{SB}}} - \frac{P_{\text{dis},i}^t \Delta t}{\eta_{\text{dis}} E_{\text{SB}}}, \tag{12}$$

where η_{ch} and η_{dis} are charging and discharging efficiencies, E_{SB} is the nominal capacity, and Δt is the time step. SoC is bounded as:

$$\text{SOC}_{\min} \le \text{SOC}_i^t \le \text{SOC}_{\max}, \tag{13}$$

with power limits $0 \le P_{\text{ch},i}^t \le P_{\text{ch}}^{\max}$ and $0 \le P_{\text{dis},i}^t \le P_{\text{dis}}^{\max}$, ensuring non-simultaneous charging and discharging All stationary battery parameters appearing in this paper, including capacity, efficiency, power limits, and SoC bounds, are adopted from [13].

2) EV Availability and Interaction: EVs connected to site i form the set $\mathcal{V}_i(t)$, whose composition varies stochastically with user behavior. Following the probabilistic model in [14], each EV e is characterized by arrival T_e^{arr}, departure T_e^{dep}, and a presence indicator $\delta_e^t = \mathbb{1}[t \in [T_e^{\text{arr}}, T_e^{\text{dep}})]$. The total usable reserve energy from the connected fleet is:

$$E_i^{\text{EV}}(t) = \sum_{e\in\mathcal{V}_i(t)} \big(\text{SOC}_e(t) - \text{SOC}_e^{\min}\big)^+ E_e^{\text{nom}}\, \delta_e^t, \tag{14}$$

where E_e^{nom} is the nominal capacity and $\text{SOC}_e^{\min}$ is the driver's minimum SoC requirement. The aggregate exchange from EVs to the BS load is constrained by the V2X interface limit $P_i^{\text{V2X,max}}$:

$$\sum_{e\in\mathcal{V}_i(t)} (P_{\text{dis},e}(t) - P_{\text{ch},e}(t)) \le P_i^{\text{V2X,max}}, \tag{15}$$

where $P_{\text{dis},e}$ and $P_{\text{ch},e}$ denote the discharge and charge power of vehicle e, respectively. Positive exchange indicates EVs assisting the site; negative exchange occurs when abundant stationary energy allows for EV BESS recharging, preserving readiness for later outage intervals.

3) Dynamic EV Pricing: To ensure participation while maintaining fairness, a dynamic pricing scheme adapts to the station's urgency and vehicle SoC. The compensation rate offered to vehicle e at time t is expressed as:

$$\rho_e(t) = \rho_{\text{base}}\Big[1 + \alpha_{\text{urg}} e^{-\hat{T}_i^{\text{surv}}(t)/\tau}\Big], \tag{16}$$

where ρ_{base} is the nominal price (\$/kWh) and $\hat{T}_i^{\text{surv}}(t) = E_i^{\text{bat}}(t)/\overline{P}_i$ estimates remaining backup survival time based

on mean power $\overline{P}_i$. The parameter τ controls the urgency timescale, while $\alpha_{\text{urg}} > 0$ is a tuning coefficient that increases incentives as site energy decreases. This formulation maintains bounded, continuous price evolution suitable for site-level optimization.

4) Site Power Balance: The instantaneous power balance at site i is:

$$P_i^{\text{load}}(t) = P_i^{\text{bat}}(t) + \sum_{e \in \mathcal{V}_i(t)} P_e(t) + P_i^{\text{grid}}(t), \tag{17}$$

where $P_i^{\text{load}}(t)$ is the traffic-driven consumption, $P_i^{\text{bat}}(t)$ is the battery charge/discharge power, and $\sum P_e(t)$ denotes net V2G exchange. The grid import term $P_i^{\text{grid}}(t)$ is zero during outages. This ensures that cooperation affects energy usage directly through load redistribution, yielding a consistent communication–energy interaction model.

III. Optimization Framework

To operate reliably during extended grid outages, cooperation decisions must be jointly optimized with user association, carrier activation, and the dispatch of stationary and mobile energy resources. The optimization block translates high-level cooperation logic into implementable control variables updated across multiple timescales. This section provides a compact formulation of the optimization problem, highlighting the coupling between energy, coverage, and service continuity.

The problem is formulated as a multi-objective MILP over a horizon $\mathcal{T}$. The decision vector $\boldsymbol{x}$ encompasses site modes $\gamma_{i,m}(t) \in \{0,1\}$ (where $m \in \{0,1,2,3\}$ identifies the modes defined in Sec. II-A), carrier states $z_i^{(b)}(t)$, user association $x_{i,u}(t)$, and power flows $P_i^{\text{bat}}(t), P_e(t)$. The objective function $\mathcal{J}$ balances survival time, service quality, economic costs, and system stability:

$$\begin{aligned} \max_{\boldsymbol{x}} \ \mathcal{J} = \lambda_1 T_{\text{surv}}^{\min} + \lambda_2 \sum_{t,u} w_u \frac{r_{i,u}(t)}{D_u(t)} \\ - \lambda_3 \sum_{t,i,e} \rho_e(t) P_e(t) \Delta t - \lambda_4 \sum_{t,i,m} \theta_{i,m}(t), \end{aligned} \tag{18}$$

where $T_{\text{surv}}^{\min}$ is the network-wide survival time. The second term maximizes the weighted satisfaction ratio, using priority weights w_u to protect critical traffic classes. The third term represents the total cost of V2G energy procurement based on the dynamic rate $\rho_e(t)$, and the final term $\theta_{i,m}$ is a penalty multiplier to minimize frequent mode-switching. The importance of each component is tuned via weights λ_k, which satisfy $\sum \lambda_k = 1$.

The cooperation topology and frequency activation are governed by the following mixed-integer constraints:

$$\sum_{m=0}^{3} \gamma_{i,m}(t) = 1, \tag{19}$$

$$\gamma_{i,1}(t) \le \sum_{j \in \mathcal{N}_i} \big(\gamma_{j,2}(t) + \gamma_{j,3}(t)\big), \tag{20}$$

$$\gamma_{i,2}(t) + \gamma_{i,3}(t) \le \sum_{j \in \mathcal{N}_i} \gamma_{j,1}(t)\, \mathbb{1}[\kappa_{ji} \ge \kappa_{\min}], \tag{21}$$

$$y_{ij}(t) = y_{ji}(t); \quad \sum_{j \in \mathcal{N}_i} y_{ij}(t) \le K_{\max}, \tag{22}$$

$$y_{ij}(t) \ge \gamma_{i,1}(t)\big(\gamma_{j,2}(t) + \gamma_{j,3}(t)\big), \tag{23}$$

$$\sum_{b \in \mathcal{B}_i} z_i^{(b)}(t) \ge 1 - M\gamma_{i,3}(t), \tag{24}$$

$$\sum_{b \in \mathcal{B}_i \setminus \mathcal{B}_i^{\text{low}}} z_i^{(b)}(t) \le M(1 - \gamma_{i,2}(t)). \tag{25}$$

Equation (19) ensures each site i selects exactly one operational mode m. Constraint (20) prevents a site from entering helping mode ($\gamma_{i,1}$) unless there are neighbors in the set $\mathcal{N}_i$ requiring assistance. Conversely, (21) ensures assisted or sleeping sites are covered by at least one helper j with sufficient assistance potential κ_{ji}. Cooperation links $y_{ij}(t) \in \{0,1\}$ are symmetric, limited to $K_{\max}$ per site, and activate between helping and assisted neighbors ((22)–(23)). Coupling between energy and radio states is managed by (24)–(25): deep-sleep sites ($\gamma_{i,3}$) deactivate all bands using a big-M constant, while assisted sites ($\gamma_{i,2}$) disable high-frequency carriers outside the low-band set $\mathcal{B}_i^{\text{low}}$. This restriction to low frequencies reduces power consumption while effectively narrowing the coverage radius as defined in (5). To ensure computational tractability, nonlinear terms are linearized using McCormick envelopes, yielding a Mixed-Integer Linear Program (MILP) [15].

IV. Two-Stage Real-Time Control

The optimization is decomposed into two hierarchical timescales to ensure computational efficiency and operational stability within a robust engineering framework.

1) Stage 1: Coarse-Grained Planning (15 min): This stage fixes binary cooperation modes (γ, y) to maximize the minimum network survival time. Using a planning horizon H (e.g., 6 hours), the objective levels battery depletion across sites:

$$\max_{\gamma,y} \ \min_{i \in \mathcal{N}} \frac{E_i^{\text{bat}}(t) - \sum_{\tau=t}^{t+H} \mathbb{E}[P_i^{\text{total}}(\tau)]\Delta\tau}{\mathbb{E}[P_i^{\text{total}}(t+H)]}, \tag{26}$$

where the denominator represents the expected power drain at the horizon limit. Updating these complex integer decisions on a slow loop maintains tractability while capturing long-term energy trends.

2) Stage 2: Fine-Grained Dispatch (30 s): With topology fixed by Stage 1, this stage optimizes continuous variables—user association, bandwidth, and V2G flows—using a logarithmic utility for proportional fairness:

$$\max_{\boldsymbol{x}_{sub}} \sum_u w_u \log\left(1 + \frac{r_{i,u}(t)}{D_u(t)}\right). \tag{27}$$

Algorithm 1 MSRC Two-Stage Controller

Require: $\{E_i^{\text{bat}}\}$, $\{D_u\}$, horizon H
Initialize all sites in Normal mode: $\gamma_{i,0} \leftarrow 1,\ \forall i$
while outage is ongoing **do**
  if $t \bmod 15\ \text{min} = 0$ **then** ▷ Stage 1
    Estimate traffic and EV presence δ_e^t over $[t, t+H]$
    Solve (26) to update modes γ and links y
  end if ▷ Stage 2
  Measure real-time channel and EV states
  Solve (27) for association x, band z, and power P
  Update battery SoC using measured site consumption
end while

Algorithm 1 summarizes the interaction. This separation ensures sub-second execution, making the framework suitable for real-time deployment in software-defined RAN controllers.

V. Simulation Setup

The proposed framework is evaluated through a Python-based simulator with the MILP problems solved via Gurobi 11.0. Results are averaged over 50 Monte Carlo trials with 95% confidence intervals.

1) Network and Infrastructure: We model a dense urban network of 19 macro BSs in a hexagonal layout (500 m inter-site distance) covering 4 km^2. The network serves 1,000 users, with 70% concentrated in hotspots to simulate non-uniform load. Each BS operates on four frequency bands $b \in \mathcal{B}_i$ (LTE 800, 1800, 2600 MHz and 5G NR 3700 MHz) with capacities $C^{(b)}$ of 50, 100, 120, and 500 Mbps, respectively. Power coefficients follow [10]. Sites possess 20 kWh battery storage, initialized at 80% SOC, with a 10 kW discharge limit. Parameters are detailed in Table I.

2) Traffic and EV Models: Traffic comprises four classes: emergency, voice, essential, and best-effort (2%, 15%, 50%, and 33% of the total). Each class follows the distribution in Table I. The EV fleet is modeled as a distributed resource with Poisson arrivals ($\lambda = 3$ per site). Vehicles $e \in \mathcal{V}_i(t)$ have heterogeneous capacities $E_e^{\text{nom}} \sim \mathcal{N}(60, 15)$ kWh and stays following an exponential distribution ($\mu = 3$ h). Other EV parameters are specified in Table I.

3) Optimization Framework: The MSRC controller weights are set to $(\lambda_1, \lambda_2, \lambda_3, \lambda_4) = (0.5, 0.3, 0.1, 0.1)$, prioritizing network survival and service continuity over cost minimization. The cooperation parameters are set to an assistance potential threshold $\kappa_{\min} = 0.3$ and a maximum of $K_{\max} = 3$ links per site.

TABLE I
Simulation Parameters

Network and Infrastructure	
Coop. Params	$R_{\text{coop}} = 1$km, $\kappa_{\min} = 0.3$, $R_{\text{red}} = 0.5$
Traffic distributions	
Emerg./Voice	Constant 64 kbps
Essential	LogNormal($\mu = 0, \sigma = 0.5$) [Mean 1 Mbps]
Best-Effort	LogNormal($\mu = 1.5, \sigma = 0.7$) [Mean 5 Mbps]
Electric Vehicles	
Initial SoC	$\mathcal{U}(0.5, 0.8)$
Discharge	Max 7 kW, $\text{SOC}_e^{\min} = 33\%$
Pricing	$\rho_{\text{base}} = 0.5$, $\alpha_{\text{urg}} = 2.0$, $\tau = 1.5$

TABLE II
Network Survival Time T_{surv} (Hours)

Traffic Load	**Indep.**	**Static LB**	**MSRC**
Light	3.2	4.5	**5.8**
Medium	2.5	3.5	**5.0**
Heavy	1.8	2.6	**3.7**
Avg. Gain	—	+41%	**+96%**

VI. Simulation Results

The primary performance metric is the network survival time T_{surv}, which should be maximized. Table II compares MSRC with the two baselines under three traffic intensities: light ($0.5\times$ nominal demand), medium ($1.0\times$), and heavy ($1.8\times$ peak load). Under medium traffic, MSRC achieves $T_{\text{surv}} = 5$ h, representing a 100% improvement over *Independent Operation* (2.5 h) and a 43% gain over *Static Load Balancing* (3.5 h). Similar relative gains are observed across all load profiles. The improvement stems from MSRC's ability to dynamically adapt cooperation modes γ_i: energy-rich helpers expand coverage (R_i^{eff}), while energy-poor sites offload traffic via assisted or deep-sleep modes, preventing premature battery depletion of critical nodes.

The performance gap with the static baseline highlights a fundamental limitation of conventional strategies: static schemes rely on fixed geometric rules regardless of local energy states, which often accelerates depletion in constrained nodes. In contrast, MSRC exhibits *topological plasticity*. By re-evaluating the energy and coverage trade-off every 15 minutes, the framework smooths energy consumption across the cluster and avoids the "weakest-link" failure that otherwise triggers an early network-wide blackout. This SOC-aware adaptation allows MSRC to maintain a 96% average gain over independent operation, significantly extending service availability during long-duration outages.

A. Service Continuity and QoS

Table III reports the service availability at $t = 2.5$ h, the exhaustion threshold for independent batteries. MSRC maintains 100% availability for emergency and voice traffic and serves 96% of essential flows, while best-effort traffic is intentionally degraded to 75%. This priority-aware shedding, driven by the service weights w_u and the objective multiplier λ_2 in (18), ensures that limited energy is reserved for critical connectivity. In contrast, independent operation leads to a total outage, while static load balancing leaves a significant fraction of essential and best-effort demand unsatisfied.

B. Energy Dynamics, V2G, and Cooperation Trade-offs

Figure 2 shows the evolution of battery reserves. Under independent operation, all sites fail nearly simultaneously at $t = 2.5$ h. In contrast, MSRC leverages its four operational modes γ_i to induce a heterogeneous energy profile: helper nodes accept faster depletion to offload neighbors, while

TABLE III
SERVICE QUALITY AT CRITICAL THRESHOLD ($t = 2.5$H)

Service Class	QoS Target	Indep.	Static	MSRC
Emergency (2%)	100%	0%	100%	**100%**
Voice (15%)	$> 95\%$	0%	95%	**100%**
Essential (50%)	$> 80\%$	0%	72%	**96%**
Best-Effort (33%)	$> 50\%$	0%	41%	**75%**
Network Status	—	**Offline**	**Critical**	**Stable**

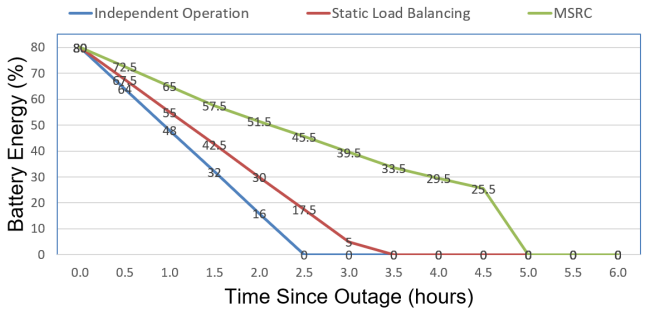

Fig. 2. Battery energy evolution under medium traffic for Independent, Static load balancing, and MSRC strategies, showing the extended backup duration achieved by MSRC.

assisted and deep-sleep nodes conserve energy for later outage stages.

The effect of dynamic V2G integration is quantified in Table IV. Under medium traffic, MSRC reaches a 5 h survival time with 61% EV utilization. The increase in EV utilization from 23% (Independent) and 35% (Static) to 61% demonstrates that the pricing scheme in (16) effectively transforms parked vehicles into active dispatched reserves. Notably, the non-zero utilization in the Independent baseline is due to individual sites utilizing local V2G energy from vehicles present at their specific locations. Load redistribution results in higher instantaneous power at helper sites, which is more than offset by savings at assisted and deep-sleep sites, reducing overall network power usage. Control overhead remains modest: average handovers per user only increase from 2.9 to 3.4, and each site performs approximately 4.2 mode switches over the entire outage (Table IV). Thus, MSRC achieves a substantial extension of T_{surv} without excessive signaling churn or new physical infrastructure.

VII. CONCLUSION AND FUTURE WORK

This paper presented the Multi-Site Resiliency Cooperative (MSRC) framework, a software-defined approach that enables neighboring base stations to form a cooperative energy cluster during grid outages. By jointly coordinating radio coverage adaptation, cooperative sleep modes, and EV-based energy support, MSRC significantly extends network survivability by up to 96% and preserves critical services without requiring additional physical infrastructure. Future work will focus on adopting more detailed and non-linear base station power models that explicitly capture the impact of scheduling, resource allocation, and link-quality variations under user migration.

TABLE IV
COMPREHENSIVE PERFORMANCE METRICS (MEDIUM TRAFFIC)

Metric	Indep.	Static	MSRC
Survival Time (h)	2.5	3.5	**5.0**
Service Continuity (%)	78	88	**96**
EV Utilization (%)	23	35	**61**
Avg. Handovers/User	—	2.9	**3.4**
Mode Switches/Site	—	0	**4.2**

Addressing these dynamics may require learning-based or heuristic control strategies, with deep reinforcement learning being a promising direction for real-time operation under stochastic traffic and EV availability.

ACKNOWLEDGMENT

This work has been supported by the project "National Center for HPC, Big Data and Quantum Computing, CN00000013 (Bando M42C – Investimento 1.4 – Avviso Centri Nazionali)" – D.D. n. 3138 of 16.12.2021, funded with MUR Decree n. 1031 of 17.06.2022.

REFERENCES

[1] F. Wang, X. Fan, F. Wang, and J. Liu, "Backup battery analysis and allocation against power outage for cellular base stations," *IEEE Transactions on Mobile Computing*, vol. 18, no. 3, pp. 520–533, 2019.
[2] L. Kehoe, "How Spain's mobile networks performed during the Iberian grid collapse," *Ookla Research*, Jun. 2025.
[3] DNV, "Energy transition outlook 2025," DNV AS, Tech. Rep., 2025.
[4] F. Hang, "Impact of electric vehicle charging demand on clean energy regional power grid control," *Energy Informatics*, vol. 8, no. 83, 2025.
[5] A. G. Papidas and G. C. Polyzos, "Self-organizing networks for 5g and beyond: A view from the top," *Future Internet*, vol. 14, no. 3, 2022.
[6] A. Martiny, M. Meo, D. Renga, and G. Vallero, "Towards resilient rans through uav integration: Landing positioning strategy during blackouts," in *2025 8th International Conference on Advanced Communication Technologies and Networking (CommNet)*, 2025, pp. 1–7.
[7] International Energy Agency (IEA), "Global ev outlook 2021," IEA, Paris, Tech. Rep., 2021, licence: CC BY 4.0. [Online]. Available: https://www.iea.org/reports/global-ev-outlook-2021
[8] D. Kikuta, H. Ikeuchi, K. Tajiri, Y. Toyama, M. Nakamura, and Y. Nakano, "Electric vehicle routing problem for emergency power supply: Towards telecom base station relief," 2024. [Online]. Available: https://arxiv.org/abs/2404.02448
[9] F. Ayaz, M. Nekovee, Z. Sheng, and N. Saeed, "Digital twin-based reinforcement learning for energy exchange among electric vehicles and base stations in a disaster-affected region," *IEEE Transactions on Intelligent Transportation Systems*, pp. 1–10, 2025.
[10] G. Vallero, G. Perin, M. Meo, M. S. Garino, S. D'Elia, and D. Vaccarono, "A new explainable power demand model for 4g lte and 5g nr base stations," in *ICC 2025*, 2025, pp. 4173–4178.
[11] 3GPP, "Study on channel model for frequencies from 0.5 to 100 ghz," 3GPP, Tech. Rep. 38.901, Dec 2019.
[12] G. Vallero, M. Meo, W. Joseph, and M. Deruyck, "Threshold-based 5g nr base station management for energy saving," *Computer Networks*, vol. 259, p. 111070, 2025.
[13] M. R. Jokar, M. Meo, G. Vallero, and D. Renga, "A battery degradation model for cost-optimized pv-bess design in telecom base stations," in *2025 IEEE 36th International Symposium on Personal, Indoor and Mobile Radio Communications (PIMRC)*, 2025, pp. 1–6.
[14] M. Latifi, A. Rastegarnia, A. Khalili, and S. Sanei, "Agent-based decentralized optimal charging strategy for plug-in electric vehicles," *IEEE Transactions on Industrial Electronics*, vol. 66, no. 5, 2019.
[15] M. Asghari, A. M. Fathollahi-Fard, S. M. J. Mirzapour Al-E-Hashem, and M. A. Dulebenets, "Transformation and linearization techniques in optimization: A state-of-the-art survey," *Mathematics*, vol. 10, no. 2, 2022.